# *Performance Assessment of Back Gated Ferroelectric STFET as a Dielectric Modulated label-Free Biosensor*

## 6.1 Introduction

In the previous chapters, we have discussed the electrostatic behavior of different proposed TFETs on a SELBOX substrate, and we have obtained the optimized TFET known as the BG-Fe-HJ-STFET in chapter-5. In this chapter, we designed a dielectric modulated biosensor using optimized TFETs (BG-Fe-HJ-STFET) for application purposes. Biosensors have gotten a lot of interest in recent years in medicine and nanotechnology, due to the invention of the first oxygen biosensor by Led and Clark in 1962 [213]. A biosensor is a biological device that is self-contained and used to detect biological components [213]-[220]. Biosensor devices have demonstrated enormous potential for use in medical diagnostics as well as other industries such as pharmaceutical, food, drinks, environmental, agricultural, and many other biotechnological industries [213]-[218]. Internet-of-Thinks (IoTs) have received much interest in the field of information and communication technology (ICT) in recent years because of the rapid growth in the development of intelligent devices that are required for a better human life [218]. It also plays a crucial part in our daily lives by allowing us to link many sorts of smart devices via wireless technology, greatly raising our life quality [218]. In recent times FET based biosensors have gained a lot of attention among worldwide researchers due to their superior properties like label-free detection, small size, rapid response, and reliability [87]. Because of their ability to identify biological species, FET-based label-free biosensors have been widely used in this regard. $I_{ON}$ sensitive field-effect transistors have also been introduced as a part of FET family, to detect the biomolecules based on

the existence of charge between the dielectric gate and the ionic solution [214], [216]-[217]. Aside from that, scaling FET (bulk MOSFET) for compactness and performance improvement of biosensor equipment results in the limitations listed below [213]-219]:

(i). The kT/q limit [subthreshold swing (SS) > 60 mV/decade] causes a significant increase in detection time,

(ii). Presence of short channel effects (SCEs),

(iii). Presence of drain-induced barrier lowering (DIBL),

(iv). Low $I_{ON}/I_{OFF}$ ratio,

(v). High power consumption due to leakage, and

(vi). Limitations related to scaling of threshold voltage with supply voltage.

To address these issues, researchers are focusing on new technology FET-based biosensors, namely TFET-based biosensors, which have low power and excellent properties due to carrier band to band tunneling and steep subthreshold swing [88]. A tunnel FET-based biosensor has been extensively investigated for this purpose and has emerged as a potential candidate due to its ability to provide better sensitivity, improved response time, and energy efficiency due to low leakage, as well as its ability to overcome all of the aforementioned issues associated with FET-based biosensors, as we have discussed in the review section of chapter-1 [87] – [100]. In addition to these, we have investigated a charge-plasma-based dielectric-modulated back gated ferroelectric heterojunction tunnel field-effect transistor on SELBOX Substrate (BG-Fe-HJ-STFET) that can be used to detect biomolecules suitable metal work-function electrodes induce P+ source and N+ drain regions for this purpose. Furthermore, within the gate dielectric, a nanogap is established to collect the biomolecules. The device's performance was evaluated in terms of the energy band diagram, e- tunneling rate, surface potential, drain current ($I_{DS}$), subthreshold swing (*SS)*, and sensitivity for this purpose. The main focus of

this chapter is on determining the effect of charge density and dielectric constant modulation on the electrical characteristics of the proposed device. In addition, the sensing capability of BG-Fe-HJ-STFET based biosensor has been analyzed. The following sections structures are as follows:

Section 6.2 contains the structure of the proposed device and simulation procedure, section 6.3 includes the fabrication feasibility of the proposed structure, section 6.4 contains the calibration of the models, whereas section 6.5 will discuss the results and their analysis and finally section 6.6 discusses the conclusion of the present chapter.

## 6.2 Device Under Study

In this section we would discuss about the specification of the device structure and simulation procedure to obtain the results.

### 6.2.1 Device Structure

Figure 6.1 depicts a 2D cross-sectional view of the BG-Fe-HJ-STFET, containing all dimension parameter symbols, and Table 6.1 gives the values of the stated symbols. In this study we have considered Ge/Si based hetero junction between source and channel [44], [82] which results in better BTBT (band to band tunneling) and lowered the subthreshold swing (*SS*) [44]. In the proposed TFET-based biosensor, a ferroelectric oxide ($k$ = 1495) is included into the gate dielectric stack directly below the gate metal [67]-[71].

### 6.2.2 Fabrication Feasibility

The proposed BG-Fe-HJ-STFET construction can be manufactured utilizing comparable steps as revealed in [109], [189]-[190]. The required fabrication process flows of the proposed BG-Fe-HJ-STFET are shown in Figure 6.2. In the first step of fabrication, we have to choose a clean p-type Si substrate on which the remaining fabrication process can be performed easily and deposited the buried oxide (BOX) SiO2 layer over the selected

substrate by using thermal oxidation process as shown in Figure 6.2 (a & b). In the next step the SELBOX gap is created by the etching of SiO2 and the growth of the n+ Ge and p− Si layers over the BOX layer by using the epitaxial method in the third step of the process flow as shown in Figure 6.2 (b & c). Then masking is pattern for the etching the Si the remaining part rather than channel and drain region then two cavities are made in p−Si layer where the p+ Ge and n+ Si are deposited by using CVD process as depicted by Figure 6.2 (d) to construct the source and channel regions of the device. After forming source and drain region, we have to dope it with required types of doping. In the succeeding advance, SiO2/ferroelectric oxide is kept as a gate oxide and then metallization and designing are done to acquire the source, drain and gate contacts then nanocavities are formed in ferroelectric oxide on both side of the gate as illustrated in Figure 6.2 (d).

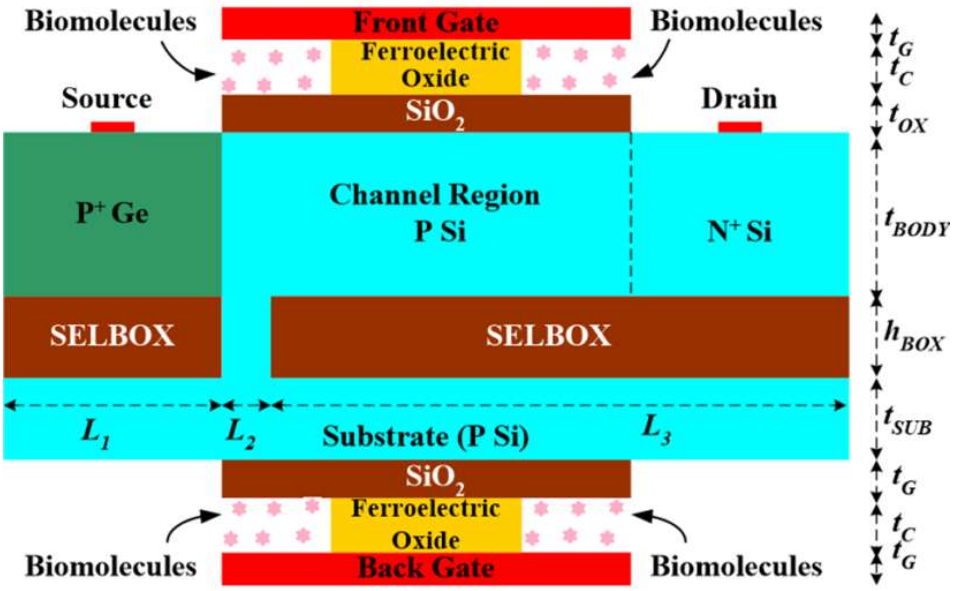


**Figure 6.1** 2-D cross-section diagram of BG-Fe-HJ-STFET based Biosensor.

**Table 6.1:** Device specifications.

| **Parameters** | **Value** | **Unit** |
|---|---|---|
| Source doping concentration ($N_S$) | $1\times10^{19}$ | $cm^{-3}$ |
| Channel doping concentration ($N_{ch}$) | $1\times10^{15}$ | $cm^{-3}$ |
| Drain doping concentration ($N_D$) | $5\times10^{18}$ | $cm^{-3}$ |
| The thickness of the channel ($t_{Si}$) | 15 | nm |
| The thickness of $SiO_2$ gate oxide ($t_{ox}$) | 1 | nm |
| Ferroelectric oxide thickness ($t_{ox}$) | 2 | nm |
| Cavities thickness ($t_c$) | 4 | nm |
| Effective Oxide Thickness (EOT) | 1.312 | nm |
| $SiO_2$ gate dielectric permittivity (ε) | 3.8 | -- |
| $HfO_2$ gate dielectric permittivity (ε) | 25 | -- |
| Gate length ($L_G$) | 40 | nm |
| Source length ($L_S$) | 30 | nm |
| Drain length ($L_D$) | 30 | nm |
| Thickness of buried oxide (BOX) ($t_{BOX}$) | 10 | nm |
| Length of SELBOX gap ($L_{BOX}$) | 2 | nm |
| Hole tunnel mass in silicon ($m_{htSi}$) | $0.24m_o$ | -- |
| Hole tunnel mass in germanium ($m_{htGe}$) | $0.044m_o$ | -- |
| Electron tunnel mass in silicon ($m_{etSi}$) | $0.20m_o$ | -- |
| Electron tunnel mass in germanium ($m_{etGe}$) | 0.082mo | -- |
| Lattice constant of Ge | 5.656 $^0$A | $^0$A |
| Lattice constant of Si | 5.429 $^0$A | $^0$A |
| Bandgap energy Ge | 0.70 eV | eV |
| Bandgap energy Si | 1.12 eV | eV |
| Electron affinity Ge | 4.01 eV | eV |
| Electron affinity Si | 4.05 eV | eV |
| Front Gate Metal Work Function (eV), $\psi_{sf}$ | 4.2 eV | eV |
| Back Gate Work Function (eV), $\psi_{sb}$ | 4.2 eV | eV |

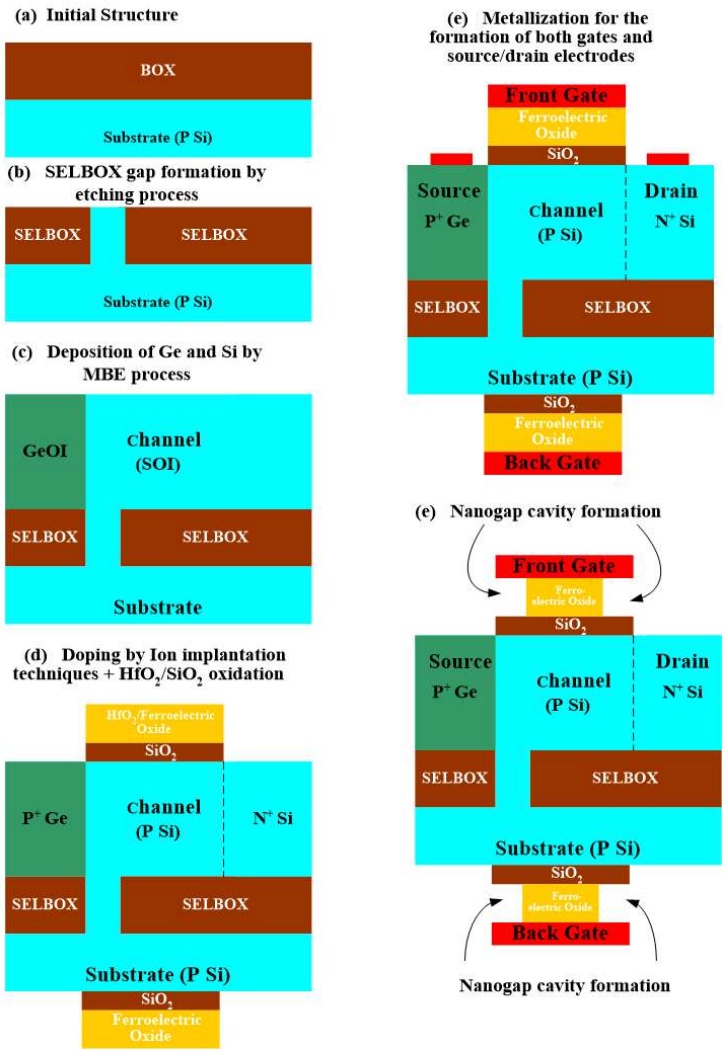


**Figure 6.2** Possible fabrication process steps of the proposed BG-Fe-HJ-STFET [109].

### 6.2.3 Calibration of the Models

The design and performance analysis of BG-Fe-HJ-STFET biosensor has been done using the commercially SILVACO ATLASTM TCAD tool [157]. In this work, the fundamental models which are used are non-local band to band tunneling (BTBT), Auger recombination model, SRH model, field-dependent mobility model, Shockley-Read-Hall generation-recombination model, and Fermi-Dirac statistics model have been used. Calibration for the used models was performed by comparing the proposed device's simulated drain current data with experimental work based on SOI TFET drain current at $V_{DS}$ = 0.5 V and $V_{DS}$ = 1.0 V, $L_G$ (gate length) = 400 nm, as shown in Figure 6.3 [158].

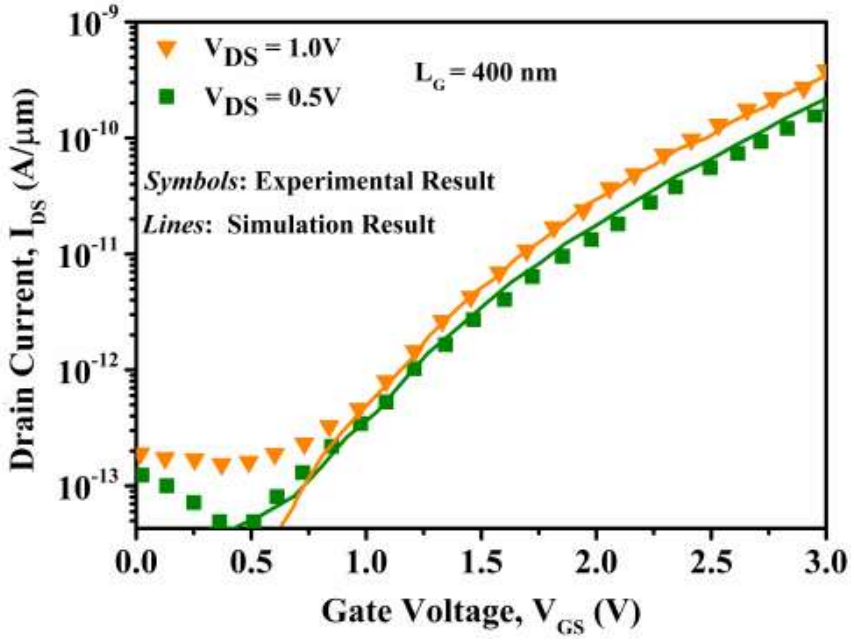


**Figure 6.3** Calibration graph of the proposed structure (BG-Fe-HJ-STFET) with prefabricated SOI TFET at $V_{DS}$ =0.5V, and $V_{DS}$ =1.0V [158].

## 6.3 Results and Discussion

This section represents the results of simulation analysis and discusses them. Negative, neutral and positive charges biomolecules are considered to analyse the response of the biosensor to immobilization of studied biomolecules. A measure of sensitivity of a dielectric modulated biosensor FET is defined as [224]-[229].

$$S_{ID} = \left| \frac{\left( S_{ID}^{Bio} - S_{ID}^{Air} \right)}{S_{ID}^{Air}} \right| \tag{6.1}$$

where, $I_d^{Bio}$ and $I_d^{Air}$ are the drain currents of the biosensor when the biomolecule filled nanogap has dielectric constant of $k > 1$, and nanogap filled with air ($k = 1$) respectively. Some physical properties are explored to reflect the fundamental function and physics of the proposed biosensor. This section describes the electrostatic behaviour of the proposed BG-Fe-HJ-STFET biosensor as the dielectric constant for neutral biomolecules and

charge density (positive and negative) for charged biomolecules vary. Figure 6.4 (a) depicts the energy band diagram in the ON-state for various neutral biomolecules with varying dielectric constants present in the biosensor cavity. It can be shown that when the dielectric constant of the biomolecule increases, the sensitive nature of the TFET based biosensor also increases, resulting in a decrease in the tunnelling barrier of the source/channel junction. The protein biomolecule, which has a higher dielectric constant of $k$ = 8, has a lower tunnelling barrier. As a result, the electric field in Figure 6.4 (b) exhibits a similar pattern. The electric field across the source/channel junction increases when the tunnelling barrier is reduced. Protein, which has the highest dielectric constant of all neutral biomolecules, has the highest peak of the electric field as shown in Figure 6.4 (b).

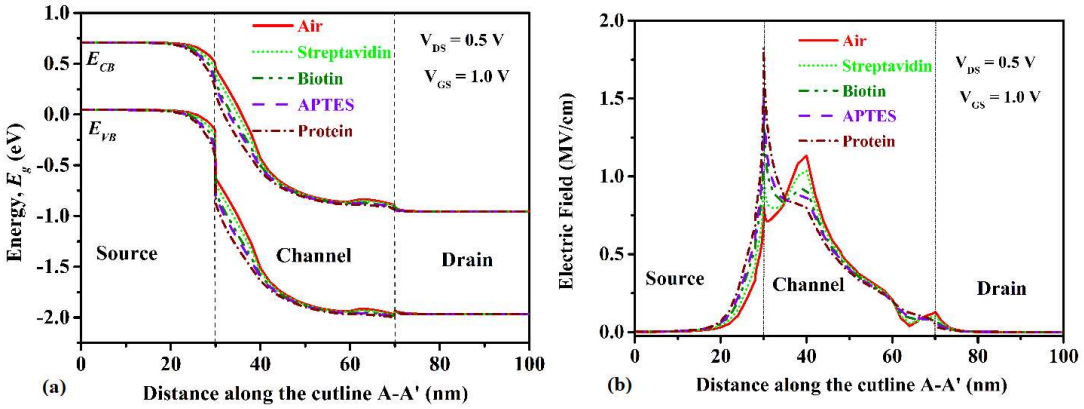


**Figure 6.4** Plots of (a) ON-state energy band diagram, and (b) 2-D Electric field of BG-Fe-HJ-STFET based biosensor at $V_{GS}$ = 1V, $V_{DS}$ = 0.5V and $t_c$ = 8 nm.

Figure 6.5 (a) depicts the graphs of surface potential of the proposed biosensor for the different biomolecules at $V_{DS}$ = 0.5 V. In the channel region surface potential is higher for high dielectric constant. Figure 6.5 (b) shows the plots of transconductance of the proposed biosensor (BG-Fe-HJ-STFET) for the studied biomolecules. The transconductance ($g_m$) of a device describes its capacity to transfer the applied gate v oltage into drain current [44]. The transconductance value for the higher dielectric contant

biomolecules such as the protein ($k$ = 8), showing higher transconductance values as compared to lower dielectric constant biomolecules. Furthermore, in the small-signal model with common source configuration, the cut-off frequency ($f_T$) is defined as the frequency at which current gain becomes unity; $f_T$ can be represented as [130], [162], [174]:

$$f_T = \frac{g_m}{2\pi\left(C_{gs} + C_{gd}\right)} \tag{6.2}$$

where $g_m$ is the transconductance, $C_{gs}$ and $C_{gd}$ are the parasitic capacitances of the proposed biosensor. Figure 6.6 (a) shows plots of cut-off frequency ($f_T$) for different biomolecules, here higher dielectric contant biomolecules shows higher cut-off frequency because of higher transconductance value. Figure 6.6 (b) shows the plots of transit time of studied neutral biomolecules at $V_{DS}$ = 0.5 V. The transit time (τ) of the device is used to calculate the sensing speed of the biosensor. Transit time is defined as the time required for charge carriers (electron or hole) to travel the distance between the device's source and drain regions. Transit time (τ) is the reciprocal of cut-off frequency ($f_T$) and is expressed as follows:

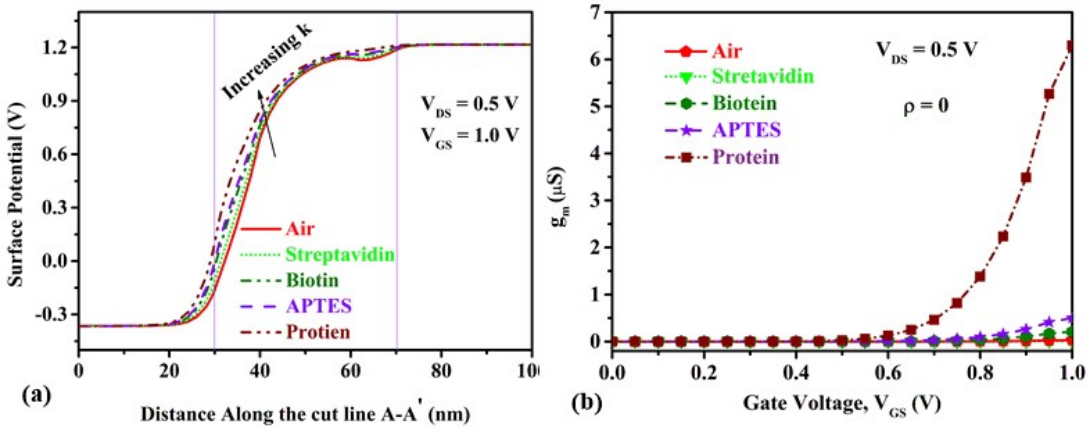


**Figure 6.5** Plots of (a) surface potential and (b) transconductance of neutral charge biomolecules of the proposed biosensor for the different biomolecules at $V_{DS}$ = 0.5 V.

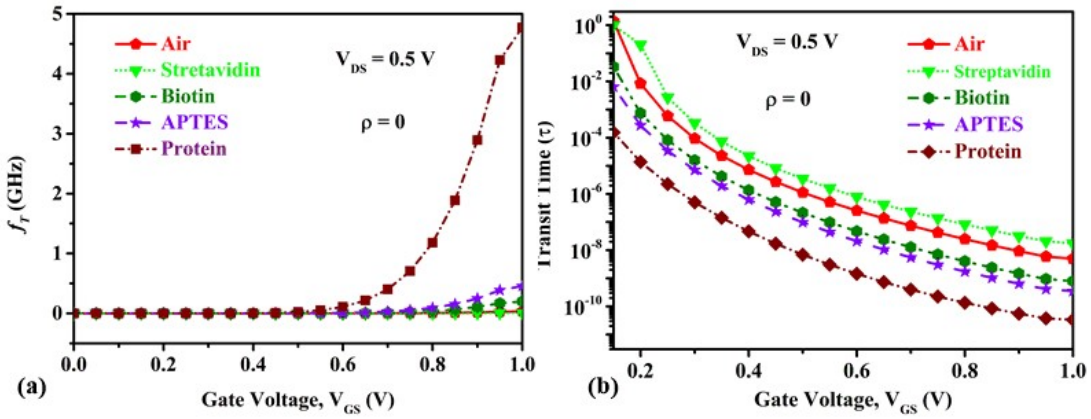


**Figure 6.6** Plots of (a) cut-off frequency and (b) transit time of neutral charge biomolecules of the proposed biosensor for the different biomolecules at $V_{DS}$ = 0.5 V.

$$\tau = \frac{1}{2\pi f_T} \tag{6.3}$$

With an increase in the dielectric constant from $k$ = 0.1 to $k$ = 8, the electron takes less time to travel from source to drain region, resulting in high speed and better biosensor response.

### 6.3.1 Impact of Charged Biomolecules

The transfer characteristics of different neutral and charged biomolecules are shown in Figures 6.7 (a) and (b), respectively. As shown in Figure 6.7 (a), the protein has a higher drain current due to increased tunnelling rate, because of smaller tunnelling barrier width and higher electric field at the source/channel. Figure 6.7 (b) depicts the tratransfer characteristics of DNA for various charge density values. In the case of DNA, there is an increase in drain current with increasing positive charge biomolecules and a decrease in drain current with increasing negative charge biomolecules [89], [95], [97]-[100]. This is due to the fact that positive charge biomolecules increase the amount of electrons, whereas negative charge biomolecules increase the number of holes in the channel region [225], [227], [229]. The sensitivity of the biosensor is described in terms of DC characteristics such as drain current ($I_{DS}$), subthreshold swing ($SS$), threshold voltage

($V_{th}$), and $I_{ON}/I_{OFF}$ sensitivity in this chapter. Sensitivity is the parameter to identify the target biomolecules with reference to air present in the cavity in the form of electrical parameters [99]. The maximum probability of detecting the targeted biomolecules is defined by higher sensitivity [96]-[100], [221]-[232]. The sensitivity of the drain current is defined by Eqn: (6.1) [15].

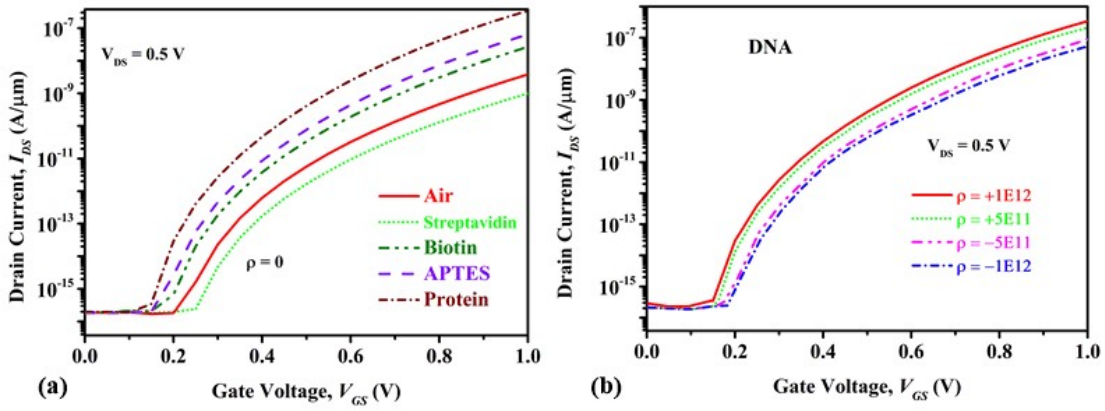


**Figure 6.7** Plots of transfer characteristics (a) neutral charge biomolecules (b) charged biomolecules (DNA) of HBG-STFET based biosensor at $V_{DS}$ = 0.5V and $t_c$ = 8nm.

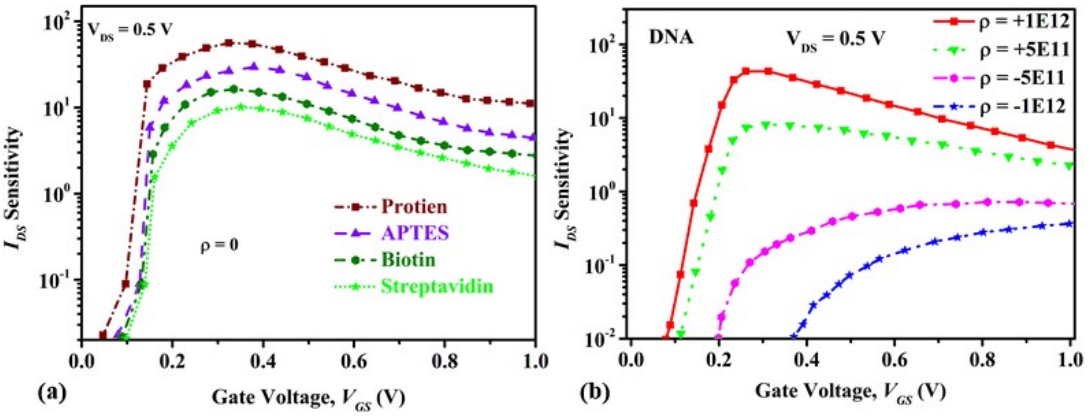


**Figure 6.8** Plots of $I_{DS}$-$V_{GS}$ Sensitivity (a) neutral charge biomolecules (b) charged biomolecules (DNA) of BG-Fe-HJ-STFET based biosensor at $V_{DS}$ = 0.5V and $t_c$ = 8nm.

Figures 6.8 (a) and (b) show the drain current sensitivity vs. gate voltage for neutral and charged biomolecules, respectively, for various dielectric constants and charge densities (positive and negative). From Figure 6.8 (a), the drain current sensitivity increases as the

biomolecule's dielectric constant increases. When compared to all other biomolecules, streptavidin has the lowest sensitivity while protein has the highest. The significant aspect of drain current sensitivity is that the highest peak occurs at the lowest gate voltage. Figure 6.8 (b) shows the drain current sensitivity for DNA for different value of charge density. For DNA, enhancement in the drain current sensitivity with increment in the positive charge biomolecule and degradation negative charge biomolecule.

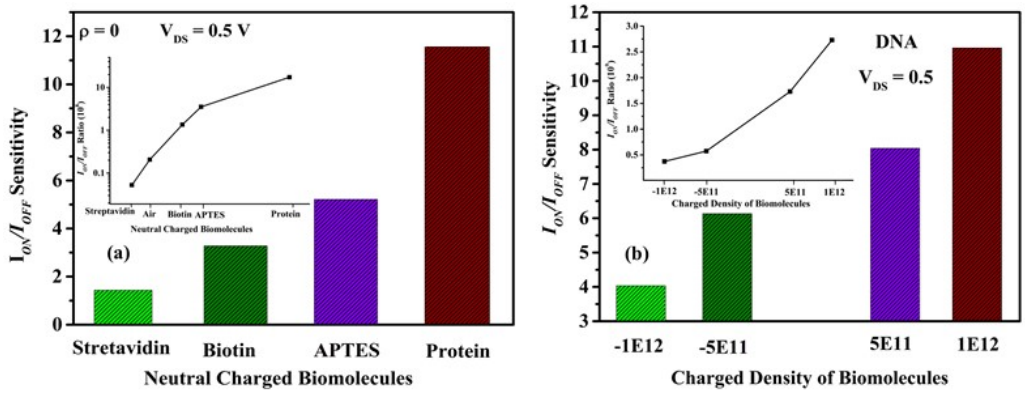


**Figure 6.9** $I_{ON}/I_{OFF}$ ratio sensitivity plot of (a) neutral charge biomolecules (b) charged biomolecules (DNA).

The $I_{DS}$ sensitivity is obtained using Eqn: (6.1), in the same way, $I_{ON}/I_{OFF}$ sensitivity is also determined. In Figure 6.9 (a), the $I_{ON}/I_{OFF}$ ratio increases as the dielectric constant within the nanogap cavity increases, because the tunnelling barrier at the source/channel interface decreases, resulting in quicker electron tunnelling rate from source to channel region [95]. So, among all neutral biomolecules, the protein ($k$ = 8) biomolecule in the nanogap cavity has the highest $I_{ON}/I_{OFF}$ ratio sensitivity. The $I_{ON}/I_{OFF}$ sensitivities of BG-Fe-HJ-STFET biosensor are depicted for five distinct values of dielectric constant ($k$ = 0.1, 2.36, 3.57, 8 and 6) with respect to different value of negative and positive charge of biomolecules as shown in Figure 6.9 (b). $I_{ON}/I_{OFF}$ sensitivities increase with magnitude of positive charge of biomolecules. However, for a fixed $k$ value proposed structure (BG-Fe-HJ-STFET) reflects more change in sensitivity than previous published work. In addition,

$I_{ON}/I_{OFF}$ sensitivity of BG-Fe-HJ-STFET sensor is plotted for different dielectric constant of biomolecules for $Q_{nf}$ =-5x10$^{11}$ cm$^{-2}$, -1x10$^{12}$ cm$^{-2}$, $Q_{pf}$ =5x10$^{11}$ cm$^{-2}$, and 1x10$^{12}$ cm$^{-2}$ in Figure 6.9 (b). With increasing the magnitude of dielectric constant, the sensitivity also increases. However, for particular positive charge of biomolecules BG-Fe-HJ-STFET reflects more change in sensitivity than a previous published work [220]-[223].

The presence of negatively charged biomolecules-$SiO_2$ interface depletion of the p-type channel, thus requiring a higher gate voltage than a neutral interface to deplete the p-type substrate, and cause reduction in channel width. The voltage balance equation of a metal-oxide-semiconductor structure is represented as [233],

$$V_{GS} = \psi_S + \phi_{MS} - \frac{qN_{bio}}{C_{ox}} \tag{6.4}$$

where $\psi_S$ is the electrostatic potential at the surface, $\phi_{MS}$ is the difference between the work functions of metal and semiconductor, $q$ is the value of electronic charge, $N_{bio}$ denotes the number of charges per unit area, and $C_{ox}$ is resultant capacitance per unit area is expressed as,

Furthermore,

$$C_{ox} = \frac{k}{t_{ox}(x)} \tag{6.5}$$

Where $k$ is the dielectric constant and $t_{ox}$ (x) is the dielectric thickness.

Considering a fixed gate voltage, as a negative charge of biomolecules increases, $\psi_s$ must decrease in order to satisfy the potential balance in (6.4), as a result drain current decreases, thus reducing the sensitivity. In (6.4), at fixed negative $N_{bio}$ and $V_{BG}$ as $k$ increases, the potential (6.6) decreases, resulting in a corresponding increase in $\psi_s$. This increases the drain current, and hence the sensitivity of biosensor. This effect is demonstrated in Figure 6.9 (b).

$$V = -\frac{qN_{bio}}{C_{ox}} \tag{6.6}$$

The constant current approach can be used to calculate the threshold voltage ($V_{th}$), with the voltage at drain current 1x10$^{-7}$A/µm treated as $V_{th}$. The $V_{th}$ sensitivity parameter is defined as [234]:

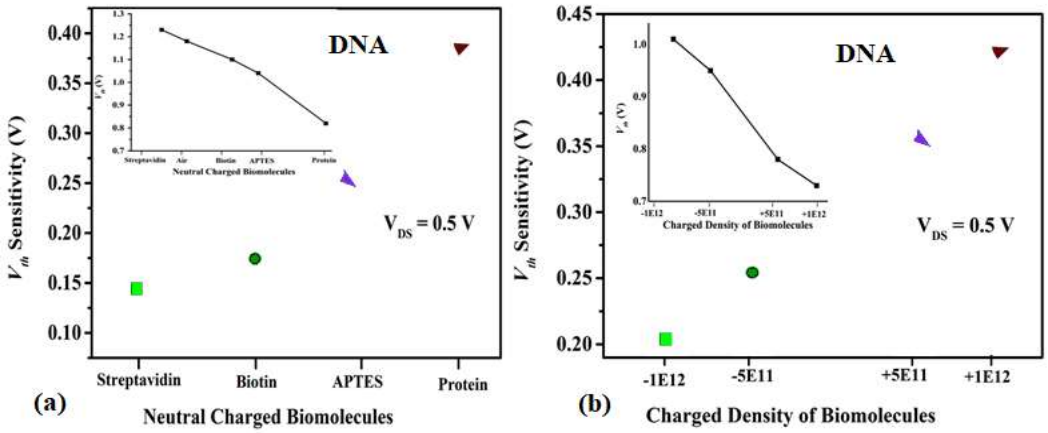


**Figure 6.10** (a) Threshold voltage ($V_{th}$) sensitivity plot of (a) neutral charge biomolecules (b) charged biomolecules (DNA).

$$\Delta V_{th} = \left|\Delta V_{th}(Air) - \Delta V_{th}(Bio)\right| \tag{6.7}$$

$\Delta V_{th}$(Air) and $\Delta V_{th}$(Bio) in this equation reflect the threshold voltages when the cavity is filled with air and biomolecules, respectively. $\Delta V_{th}$ also represents the shifting of the threshold voltage during the detection of biomolecules in air. The plot of $V_{th}$ is shown in Figure 6.10 (a) inset, where $V_{th}$ falls when the cavity is filled with biomolecules with a higher dielectric constant. As a result, the drain current reaches 1x10$^{-7}$ sooner than air. The $V_{th}$ sensitivity is calculated using Eqn: 6.7, and among all neutral biomolecules, the protein ($k$ = 8) has the highest sensitivity. Similarly, the inset in Figure 6.10 (b) reveals a higher $V_{th}$ value for more negative charge density of DNA and a lower $V_{th}$ value for more positive charge density of DNA.

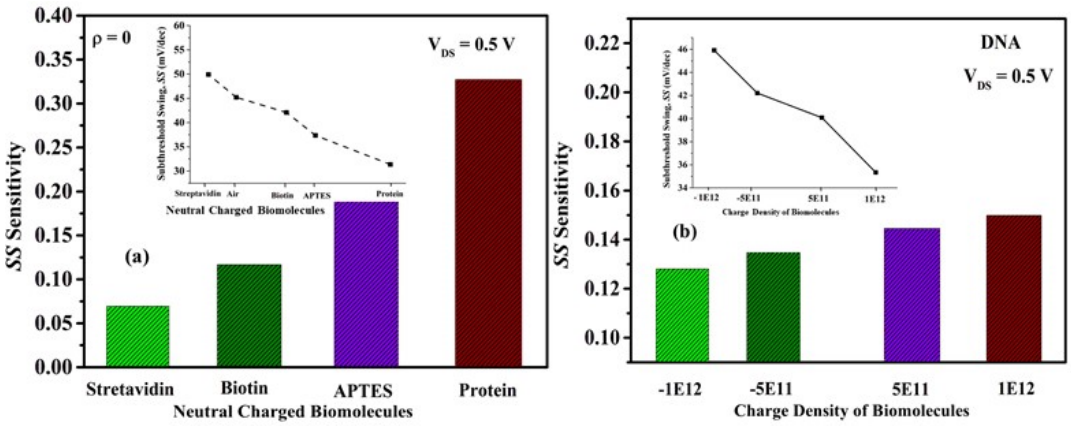


**Figure 6.11** Subthreshold swing (SS) sensitivity plot of (a) neutral charge biomolecules (b) charged biomolecules (DNA) of BG-Fe-HJ-STFET based biosensor at $V_{DS}$ = 0.5V and $t_c$ = 8nm.

SS sensitivity is important in biosensor performance since it specifies the speed with which biomolecules are detected. SS sensitivity is defined as follows [234]:

$$S_{SS} = \left| \frac{\left( S_{SS}^{Bio} - S_{SS}^{Air} \right)}{S_{SS}^{Air}} \right| \tag{6.8}$$

where $S_{SS}^{Bio}$ and $S_{SS}^{Air}$ represent the *SS* when the biosensor cavity is filled with biomolecules (neutral and charged) and air, respectively.

The SS sensitivity for neutral and charged biomolecules is depicted in Figures 6.11 (a) and (b). A lower *SS* value improves the detection potential and electrical response of the BG-Fe-HJ-STFET biosensor. In Figure 6.11 (a), it is evident that increasing the dielectric constant of biomolecules from air ($k$ = 1) to protein ($k$ = 8) reduces *SS*. It means that when the dielectric constant of the biomolecule increases, so does sensitivity. Similarly, Figure 6.11 (b) depicts the charge biomolecule (DNA) for various charge densities; the SS of the device increases as negative charge density increases and decreases as positive charge density increases. In addition, changing the charge density from negative to positive improves the suggested biosensor's SS sensitivity. Table 6.2 compares the proposed work to two other published works, referred to as [220] and [250].

**Table 6.2:** Comparison of the sensitivity with the ref. [217],[220].

| **Parameters** | **This Work (Protein)** | **[220]** | **[250]** |
|---|---|---|---|
| $I_{ON}$ Current | $4.25x10^{-6}$ A/μm | $3.50x10^{-6}$ A/μm | $4.10x10^{-6}$ A/μm |
| $I_{ON}/I_{OFF}$ Sensitivity | $4.2x10^{11}$ | $2.88x10^{11}$ | $1.31x10^{8}$ |
| $V_T$ Sensitivity | 0.38V | 1.50 V | 1.65 V |
| SS Sensitivity | 0.34 | ------ | ----- |

## 6.4 Conclusion

Proposed $SiO_2$/Ferroelectric oxide stacked back-gated Ge/Si heterojunction TFET on SELBOX substrate (BG-Fe-HJ-STFET) based dielectric modulated label-free biosensor hased been designed in chapter. The SELBOX substrate has been used in the proposed TFET-based biosensor to improve the $I_{ON}/I_{OFF}$ sensitivity. Four cavities have been created in the ferroelectric gate-oxide of the studied TFET, and they contain the biomolecules to be sensed using the gate-dielectric modulation principle. The $I_{ON}/I_{OFF}$ sensitivity, subthreshold swing sensitivity and threshold voltage sensitivity parameters of the proposed BG-Fe-HJ-STFET structure have been thoroughly investigated considering different biomolecules. The proposed BG-Fe-HJ-STFET structure outperforms some recently reported TFET-based biosensors in terms of $I_{ON}/I_{OFF}$ sensitivity, subthreshold swing sensitivity and threshold voltage sensitivity. The proposed BG-Fe-HJ-STFET structure is shown to have the higher current sensitivity ($\sim 4.2 \times 10^{11}$) and threshold voltage sensitivity (0.38V) values over some recently reported TFET based biosensors.